Circular Polarization Excitation and Detection in ^{14}N NQR

Y. K. Lee, H. Robert, and D. K. Lathrop

Quantum Magnetics, Inc., 7740 Kenamar Court, San Diego, California 92121

E-mail: Young.Lee@qm.com; Hector.Robert@qm.com; Dan.Lathrop@qm.com

Circular polarization excitation and detection of ^{14}N NQR signal are reported. A theoretical model is presented in terms of fictitious spin-1/2 operators and is compared to experiments performed on a powder crystalline sample of RDX. It is shown that in spin-1 systems with finite asymmetry—unlike previously reported NMR and symmetric spin-3/2 NQR systems (Chen *et al., J. Magn. Reson.* 54, 324–327, 1983; Weber and Hahn, *Phys. Rev.* 120, 365–375, 1960)—the circular polarization nature of the signal is due to powder orientation effects in polycrystalline samples. Sensitivity improvements up to a factor of $\sqrt{2}$ are reported using the same hardware and switching modes from linear polarization to circular polarization; this also is shown to result from the polycrystalline nature of the samples. © 2001 Academic Press

1. INTRODUCTION

Circular polarization (CP) excitation was first used in NQR to show that transitions between double degenerate $\Delta m = \pm 1$ transitions in an axially symmetric spin-3/2 system could be independently excited by switching the circular polarity of the excitation field (*8*). It was later shown that in NMR, by incorporating CP detection and excitation, the power requirements could be reduced by a factor of 2 while the sensitivity is increased by a factor of $\sqrt{2}$ (*3*). Subsequently, birdcage coil designs which provide homogeneous RF intensities while incorporating quadrature excitation modes have been widely used in NMR imaging (*4, 5*). This increase in excitation efficiency and sensitivity is shown to be a direct result of the inherent circular polarization nature of NMR signals. In pure NQR, however, the signal is inherently linearly polarized (*1*). In addition, the effective excitation field depends on the relative orientation of the electric field gradient (EFG) principal axis system (PAS) frame and excitation field in the coil. Thus in NQR, unlike NMR, it is not at all obvious that circular polarization excitation will result in a circularly polarized signal or that there would be any improvements in the signal-to-noise ratio (SNR). Researchers at the Naval Research Laboratory, however, have recently reported improved sensitivity in ^{14}N NQR using a birdcage coil tuned to CP excitation and detection (*6*).

In this report, we present theoretical calculations, computer simulations, and experimental results examining CP excitation in spin-1 NQR and how it compares with linear polarization (LP) excitation. We show that both the CP nature of the signal and the increased SNR are due to the powder orientation effects in a polycrystalline system. All experiments reported in this paper are of ^{14}N NQR from a powder crystalline sample of RDX (hexahydro, 1,3,5-trinitro, 1,3,5-triazine: $C_3H_5N_6O_6$). Signal amplitudes are compared between numerical simulations and single-pulse and two-pulse spin echo experiments.

2. THEORY

The theory presented in this section will use the fictitious spin-1/2 operators introduced by Vega and Pines (*7*) and modified for NQR by Cantor and Waugh (*2*). The notations and conventions used will follow closely those of Ref. (*2*). Two frames of reference are designated: $\{x', y', z'\}$ for the laboratory frame and $\{x, y, z\}$ for the EFG PAS frame. The angular momentum spin operators in these respective frames are then designated as $\{I_{x'}, I_{y'}, I_{z'}\}$ and $\{I_x, I_y, I_z\}$.

In the EFG PAS frame, the nuclear quadrupole Hamiltonian H_Q may be written as

$$H_Q = \frac{1}{3} \omega_Q \left[3I_z^2 - I(I+1) + \frac{\eta}{2}(I_+^2 + I_-^2) \right], \quad [1]$$

where the strength of the quadrupole coupling constant is given by ω_Q. Substituting for the fictitious spin-1/2 operators defined in the appendix, H_Q may be written in three equivalent forms:

$$H_Q = \omega_p^a I_{p,3} + \omega_p^b I_{p,4}, \quad p = x, y, z, \quad [2]$$

where

$$\omega_x^a = \omega_Q(3+\eta)/3, \quad \omega_x^b = -\omega_Q(1-\eta)/3, \quad [3]$$

$$\omega_y^a = -\omega_Q(3-\eta)/3, \quad \omega_y^b = -\omega_Q(1+\eta)/3, \quad [4]$$

$$\omega_z^a = -2\omega_Q\eta/3, \quad \omega_z^b = 2\omega_Q/3. \quad [5]$$

The set of frequencies ω_p^a corresponds to the three spin-1 NQR transition frequencies.

The RF Hamiltonian written in the lab frame consists of two orthogonal B_1 fields along the x' and y' directions, with the two components oscillating with frequency ω and a relative phase ϕ_r:

$$H_{RF}^{Lab}(t) = \omega_1[\cos(\omega t)I_{x'} + \cos(\omega t + \phi_r)I_{y'}]. \qquad [6]$$

The nutation frequency is defined as

$$\omega_1 = \gamma_N B_1, \qquad [7]$$

where γ_N is the gyromagnetic ratio of ^{14}N and B_1 is the strength of the RF magnetic field. Such fields may be created by using two independent coils or a single coil such as a birdcage coil, where two orthogonal modes can be excited with a well-defined relative phase.

Using the fictitious spin-1/2 operator definitions in the Appendix and a coordinate transformation from the laboratory to the EFG PAS frame, the RF Hamiltonian may be written as

$$\begin{aligned} H_{RF}(t) = 2\omega_1\{&[R_{11}\cos(\omega t) + R_{12}\cos(\omega t + \phi_r)]I_{x,1} \\ &+ [R_{21}\cos(\omega t) + R_{22}\cos(\omega t + \phi_r)]I_{y,1} \\ &+ [R_{31}\cos(\omega t) + R_{32}\cos(\omega t + \phi_r)]I_{z,1}\}, \qquad [8] \end{aligned}$$

where the variables R_{ij} are the elements of a general rotation matrix that define the orientation of the EFG PAS frame with respect to the laboratory frame. The rotation matrix may be written using the Euler angles α, β, and γ as consecutive rotations about the z', y', and z' axes in the laboratory frame:

$$R(\alpha, \beta, \gamma) = R_{z'}(\alpha) R_{y'}(\beta) R_{z'}(\gamma), \qquad [9]$$

where

$$R_{z'}(\alpha) = \begin{bmatrix} \cos\alpha & \sin\alpha & 0 \\ -\sin\alpha & \cos\alpha & 0 \\ 0 & 0 & 1 \end{bmatrix}, \qquad [10]$$

$$R_{y'}(\beta) = \begin{bmatrix} \cos\beta & 0 & -\sin\beta \\ 0 & 1 & 0 \\ \sin\beta & 0 & \cos\beta \end{bmatrix}, \qquad [11]$$

$$R_{z'}(\gamma) = \begin{bmatrix} \cos\gamma & \sin\gamma & 0 \\ -\sin\gamma & \cos\gamma & 0 \\ 0 & 0 & 1 \end{bmatrix}. \qquad [12]$$

Under RF radiation, the isolated spin NQR system is described by the total Hamiltonian,

$$H(t) = H_Q + H_{RF}(t). \qquad [13]$$

The Hamiltonian may be approximated in an interaction frame where the main Hamiltonian term H_Q has been removed. Using the transformation operator

$$U(t) = e^{-iH_Q t}, \qquad [14]$$

the Hamiltonian in the interaction frame becomes

$$\tilde{H}(t) = U(t)^{-1}H(t)U(t) - iU(t)^{-1}\frac{d}{dt}U(t) \qquad [15]$$

$$= U(t)^{-1}H_{RF}(t)U(t). \qquad [16]$$

From the commutation rules in Eq. [44], the interaction frame transformation of the $I_{p,1}$ operators, where $p = \{x, y, z\}$, can be shown to be

$$e^{iH_Q t}I_{p,1}e^{-iH_Q t} = I_{p,1}\cos(\omega_p^a t) - I_{p,2}\sin(\omega_p^a t). \qquad [17]$$

This transformation shows that, in the interaction frame, an RF magnetic field applied along the p PAS frame axis will lead to time-independent or "on resonance" terms only at ω_p^a radiation frequencies. Furthermore, the dynamics will also be confined to operators within the "p" subspace. The p axis when radiating on resonance at ω_p^a will be referred to as the "excitation axis." For simplicity, we assume that the RF field is being applied along the z axis at the ω_z^a resonance frequency; the final results are the same for radiation along the other two axes at their respective resonant frequencies but with more complicated functional forms for the signals. The effective Hamiltonian in the interaction frame can then be approximated to lowest order as the time averaged Hamiltonian:

$$\bar{\tilde{H}} = \omega_1\sin\beta[\cos\gamma I_{z,1} + \sin\gamma(I_{z,1}\cos\phi_r + I_{z,2}\sin\phi_r)]. \qquad [18]$$

Using the same coil system for detection, the signals for the two modes along x' and y' are detected independently in quadrature. Quadrature detection requires two observables 90° out of phase for each of the two detection modes. Written in complex notation, the observables in the lab frame for the two RF modes become

$$O_1^{Lab}(t) = I_{x'}[\cos(\omega t) + i\sin(\omega t)],$$
$$O_2^{Lab}(t) = I_{y'}[\cos(\omega t) + i\sin(\omega t)], \qquad [19]$$

where the subscripts 1 and 2 correspond, respectively, to the RF modes with the B_1 along the x' and y' lab frame axes. Following arguments similar to those used to obtain $\bar{\tilde{H}}$ in Eq. [18], the time-independent observables in the interaction frame with $\omega = \omega_z^a$ may be written using fictitious spin-1/2 operators as

$$\tilde{O}_1 = \sin \beta \cos \gamma (I_{z,1} - iI_{z,2}),$$

$$\tilde{O}_2 = \sin \beta \sin \gamma (I_{z,1} - iI_{z,2}). \qquad [20]$$

The signal in each of the modes is then defined as

$$S_i(t) = \text{tr}[\tilde{\rho}(t)\tilde{O}_i], \qquad [21]$$

where $\tilde{\rho}(t)$ is given by the evolution of the initial density operator $\tilde{\rho}_0$ under the effective Hamiltonian:

$$\tilde{\rho}(t) = e^{-i\bar{H}t}\tilde{\rho}_0 e^{i\bar{H}t}. \qquad [22]$$

3. EXAMPLES

Using the formalism from the previous section, we will now consider specific calculations of CP and LP excitation signals and examine their dependence on the orientation of the excitation fields and their relative SNR. The Euler angle γ can be interpreted as the orientation of the projection of the excitation axis (the z axis in our examples) on to the laboratory $x' - y'$ plane, and it is the signal dependence on γ that is fundamentally different in CP and LP cases.

Circularly polarized excitation fields may be obtained by setting

$$\phi_r = \frac{\pi}{2}. \qquad [23]$$

The effective Hamiltonian in the interaction frame then becomes

$$\bar{H} = \omega_1^{CP}[I_{z,1}\cos \gamma + I_{z,2}\sin \gamma], \qquad [24]$$

where

$$\omega_1^{CP} = \omega_1 \sin \beta \qquad [25]$$

is the effective nutation frequency for CP excitation. In the high temperature approximation, given that $I_{z,4}$ does not participate in the dynamics, the initial density operator can be assumed to be

$$\tilde{\rho}_0 = I_{z,3}. \qquad [26]$$

The time evolution of the density operator then becomes

$$\tilde{\rho}(t) = I_{z,3}\cos(\omega_1^{CP}t) + [I_{z,1}\sin \gamma - I_{z,2}\cos \gamma]\sin(\omega_1^{CP}t), \qquad [27]$$

and the signals in the two modes given by Eq. [21] may be written as

TABLE 1
Circular Polarization Excitation

γ	S_1 amplitude	S_2 amplitude	ω_{1eff}
0	$\frac{i}{2} \sin \beta$	0	$\omega_1\sin\beta$
$\pi/4$	$\frac{1}{4}(1 + i)\sin \beta$	$\frac{1}{4}(1 + i)\sin \beta$	$\omega_1\sin\beta$
$\pi/2$	0	$\frac{1}{2} \sin \beta$	$\omega_1\sin\beta$

$$S_1^{CP}(t) = \frac{i}{2} \sin \beta \cos \gamma \, e^{-i\gamma}\sin(\omega_1^{CP}t),$$

$$S_2^{CP}(t) = \frac{i}{2} \sin \beta \sin \gamma \, e^{-i\gamma}\sin(\omega_1^{CP}t). \qquad [28]$$

Both $S_1^{CP}(t)$ and $S_2^{CP}(t)$ have a γ dependence in the signal amplitude and phase with the phase being identical in both:

$$\phi = \frac{\pi}{2} - \gamma. \qquad [29]$$

Thus the signal from CP excitation of a single crystal sample with any orientation is *linearly polarized* rather than circularly polarized with the axis of linear polarization along the excitation axis. However, because the phase and amplitude of the single crystal signal vary with the orientation of the z axis projection on the $x' - y'$ plane, even though each crystallite contributes a linear polarized signal, combinations of crystallite signals can result in a signal that is circularly polarized. Table 1 lists the signal amplitudes for CP excitation in each coil for three different γ orientations. The signals $S_1(t)$ and $S_2(t)$ from crystallites with $\gamma = 0$ and $\gamma = \pi/2$ are out of phase by 90°; thus their combined signal, as well as the combined signal of any crystallite pair with a difference in γ of 90°, will result in a circularly polarized signal. The circular polarization nature of a powder crystalline sample may be shown by integrating the signals in Eq. [28] over γ. Defining the γ integrated signal as

$$\langle S_i \rangle_\gamma = \frac{1}{2\pi} \int_0^{2\pi} S_i d\gamma, \qquad [30]$$

we obtain

$$\langle S_1 \rangle_\gamma = \frac{i}{4} \sin \beta \sin(\omega_1^{CP}t),$$

$$\langle S_2 \rangle_\gamma = \frac{1}{4} \sin \beta \sin(\omega_1^{CP}t), \qquad [31]$$

with the full powder averaged signal for each mode given by an additional integral over β,

$$\langle S_i \rangle_{\gamma,\beta} = \frac{1}{2} \int_0^\pi \langle S_i \rangle_\gamma \sin \beta \, d\beta. \qquad [32]$$

The signals for the two orthogonal modes in Eq. [31] are 90° out of phase from one another, showing that the γ averaged NQR signal (and consequently the full powder averaged signal) from CP excitation is *circularly polarized.*

The signal from LP excitation may be calculated either by setting the phases on the two orthogonal coils to be equal or by removing one of the coils (or disconnecting one of the coil modes). If we remove the coil along the y' direction, the effective Hamiltonian becomes

$$\bar{\bar{H}} = \omega_1^{LP1} I_{z,1}, \qquad [33]$$

where

$$\omega_1^{LP1} = \omega_1 \sin \beta \cos \gamma. \qquad [34]$$

The density operator and signal for the single coil linear polarization system may then be calculated as

$$\tilde{\rho}(t) = I_{z,3} \cos(\omega_1^{LP1} t) - I_{z,2} \sin(\omega_1^{LP1} t), \qquad [35]$$

$$S_1^{LP}(t) = \frac{i}{2} \sin \beta \cos \gamma \sin(\omega_1^{LP1} t). \qquad [36]$$

Alternatively, if we keep both coils and set the phase offsets in the coils to be

$$\phi_r = 0, \qquad [37]$$

the effective Hamiltonian and observable may be written as

$$\bar{\bar{H}} = \omega_1^{LP2} I_{z,1}, \qquad [38]$$

TABLE 2
Dual Coil Linear Polarization Excitation

γ	S_1 amplitude	S_2 amplitude	ω_{1eff}
0	$\frac{i}{2} \sin \beta$	0	$\omega_1 \sin \beta$
$\pi/4$	$\frac{i}{2\sqrt{2}} \sin \beta$	$\frac{i}{2\sqrt{2}} \sin \beta$	$\sqrt{2}\, \omega_1 \sin \beta$
$\pi/2$	0	$\frac{i}{2} \sin \beta$	$\omega_1 \sin \beta$

TABLE 3
Single Coil Linear Polarization Excitation

γ	S_1 amplitude	S_2 amplitude	ω_{1eff}
0	$\frac{i}{2} \sin \beta$	0	$\omega_1 \sin \beta$
$\pi/4$	$\frac{i}{2\sqrt{2}} \sin \beta$	0	$\frac{1}{\sqrt{2}} \omega_1 \sin \beta$
$\pi/2$	0	0	0

where

$$\omega_1^{LP2} = \omega_1 \sin \beta (\cos \gamma + \sin \gamma). \qquad [39]$$

The density operator then becomes

$$\tilde{\rho}(t) = I_{z,3} \cos(\omega_1^{LP2} t) - I_{z,2} \sin(\omega_1^{LP2} t), \qquad [40]$$

and signals for the two modes may be written as

$$S_1^{LP}(t) = \frac{i}{2} \sin \beta \cos \gamma \sin(\omega_1^{LP2} t),$$

$$S_2^{LP}(t) = \frac{i}{2} \sin \beta \sin \gamma \sin(\omega_1^{LP2} t). \qquad [41]$$

As in the case for CP excitation, the single crystal signals in the two channels for dual mode LP excitation have identical phases so both single and dual mode LP excitation result in linearly polarized signals for a given orientation. Unlike the case for CP excitation, however, the phases of the signals in the two coils for dual mode LP excitation are independent of crystallite orientation; thus the NQR signal will remain linearly polarized even for the powder averaged signal.

We will now examine the nutation frequencies and relative SNRs for single crystal orientations. The signal amplitudes (the time-independent components of the signals) and the effective nutation frequencies for different γ orientations are listed in Tables 1–3.

For single coil LP excitation, the maximum effective nutation frequency $\omega_{1eff} = \omega_1 \sin \beta$ is obtained for $\gamma = 0$, while for the double coil system, the maximum $\omega_{1eff} = \sqrt{2}\, \omega_1 \sin \beta$, is obtained for $\gamma = \pi/4$. For CP excitation, the effective nutation frequency $\omega_{1eff} = \omega_1 \sin \beta$ is independent of γ. Thus, given a single crystal sample, an orientation can be found where the nutation rate is a factor of $\sqrt{2}$ larger for LP excitation compared to CP excitation for the same power input. This is a direct result of the inherent LP nature of NQR and is converse of what is observed in NMR where the inherent CP nature of NMR results in a $\sqrt{2}$ increase in nutation frequency for CP excitation.

Likewise, the maximum signal intensities for LP excitation are obtained at $\gamma = 0$ and $\gamma = \pi/4$ for the single and dual mode
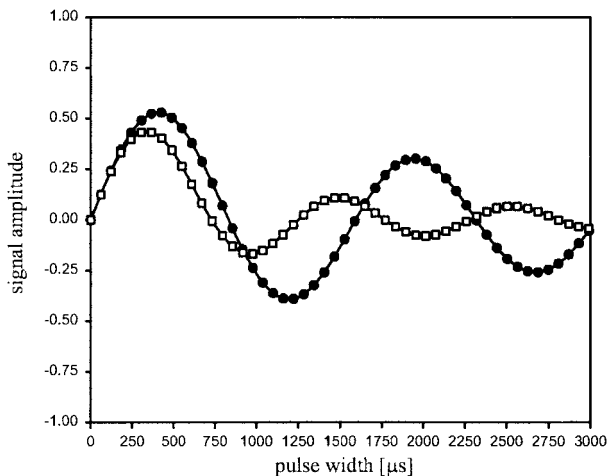
FIG. 1. Simulated powder averaged signal amplitudes for (●) CP and (□) LP excitation as a function of the RF excitation pulse width for $\omega_1/2\pi = 984$ Hz. The signals from both excitation modes are combined to obtain the overall signal intensities. The signals are normalized to the maximum signal obtainable from a single crystal with the same number of nuclei.

cases, respectively. Although the maximum signal intensity is larger by $\sqrt{2}$ in the dual mode case, since the noise also increases equally, the overall maximum SNR stays the same. For CP excitation, the maximum signal is obtained at $\gamma = \pi/4$ with signals in both the real and the imaginary channels. For this orientation, the complex magnitude of the signal amplitude is identical to the magnitude of the maximum dual mode LP excited signal amplitude; thus the maximum CP excited SNR for a single crystal is the same as those of the LP excitation cases.

The improvements in sensitivity then come from averaging signals from a polycrystalline sample. Figure 1 shows simulated curves of powder averaged signal amplitudes as a function of the RF excitation pulse width using $\omega_1/2\pi = 984$ Hz. The signal amplitude axis is normalized to the maximum signal obtainable for a single crystal with the same number of nuclei. The LP and CP modes were switched by changing ϕ_r in Eq. [6]. For a powder sample, signals for both LP and CP excitation can be detected in only one of the two complex channels. The signals from both excitation modes along x' and y' are combined to obtain the final signal amplitudes. The maximum amplitudes for the circular and linear polarization experiments are 0.53 and 0.44, respectively, corresponding to a relative signal amplitude (and SNR) of ~ 1.2. The optimum pulse for CP excitation, however, was longer by about 15%; thus even for a powder sample, the shorter optimum pulse widths observed in CP NMR are not seen in NQR.

4. HARDWARE

A coil design commonly used in NMR to produce and detect circularly polarized signals is the birdcage coil. The implementation of the coil and other hardware components will be described briefly in this section; further details will be presented in a later publication. The low pass version of the birdcage coil is shown schematically in Fig. 2. The low pass design was chosen for our application because at the RDX ^{14}N NQR frequencies ranging from 1.9 to 5.2 MHz, fewer capacitors would be required compared to other designs. The number of legs can be any even number greater than four, with more legs producing more uniform fields at the cost of greater complexity. An eight-leg design, which is the simplest design that allows fairly easy asymmetry compensation, was chosen.

The coil has overall dimensions of 32.8 cm in diameter and 45.5 cm in length. These dimensions follow approximately those used for coil designs in our current research on small package scanners for explosive detection. Two circular strips of copper at each end of the coil are connected by linear copper strips joined by capacitors. The width of these strips, 6.4 cm, was determined by two- and three-dimensional finite element modeling to maximize the coil Q at 3.4 MHz. The modeling work showed that our coil should obtain a Q of 870; a similarly sized solenoid coil would achieve a Q of 1600.

In order to achieve the highest Q possible, the birdcage coil is constructed from sheet copper and low loss porcelain capacitors. A cylindrical copper shield with a diameter of 65.5 cm (twice the coil diameter) is centered around the coil. The bottom is sealed with a circular sheet of copper and the top is sealed with a removable sheet of copper to allow access to the coil center. Guides are then installed to position the coil in the center of the shield and to maintain symmetry. The two orthogonal modes of the birdcage coil are inductively coupled by two small coils connected to feedthrough BNC connectors placed on the shield separated by 90°. By changing the size and position of these coupling coils, the impedance matching of the two modes to the external connections can be adjusted. A final Q of 800 was measured for the full coil system which is slightly lower than the numerical predictions.

A schematic of the spectrometer is shown in Fig. 3. The spectrometer including the pulse programmer, data acquisition board, and pulse programming software were all developed at Quantum Magnetics, Inc. A 200-MHz Pentium II based indus-
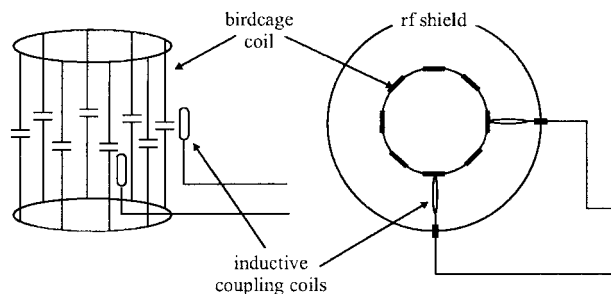
FIG. 2. Low pass birdcage coil schematics shown in side and top views. The coil design uses copper strips for two circular conductors the eight linear capacitor rungs. The RF is inductively coupled to the main coil which is encased in a copper RF shield.
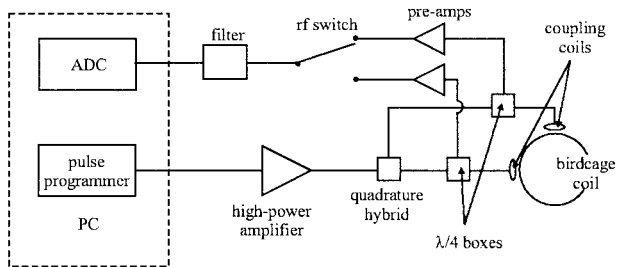
FIG. 3. Circular polarization spectrometer. A quadrature hybrid placed after the high power amplifier splits the RF power to drive the two modes of the birdcage coil. A switch is used to acquire the signals from the two channels in sequential experimental scans.

trial PC using the QNX operating system is used to run the spectrometer software. The circularly polarized field is produced by driving the two modes of the birdcage coil in quadrature. This is done by using a quadrature hybrid (Fig. 4) between the high power RF amplifier and the coil. Terminals C1 and C2 of the hybrid are connected through $\lambda/4$ duplexers to the inductive coupling coils inside the RF shield. To drive the birdcage coil in LP mode, the C2 terminal and one of the coupling coils are both terminated by 50-Ω loads; the RF power from C1 then drives one of the birdcage coil modes. The spectrometer used for the experiments discussed in this paper incorporated only one ADC; thus the signals from the two CP modes are detected in consecutive experiments and then combined.

5. EXPERIMENTAL AND SIMULATION RESULTS

The experiments were run on a plasticized powder crystalline sample of RDX placed at the center of the shielded birdcage coil tuned to 3.41 MHz. Circular polarization excitation was induced by driving the two modes of the birdcage coil in quadrature; linear polarization excitation was induced by driving only one of the two modes. By measuring the B_1 field amplitudes in CP mode using a small coupling coil placed at the center of the birdcage coil, we obtained $\omega_1/2\pi = 984$ Hz
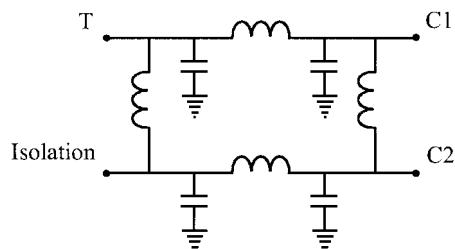
FIG. 4. Quadrature hybrid. The RF input is at the T terminal. The output RF at the C1 and C2 terminals has a relative phase shift of 90°. To drive the birdcage coil in LP mode, a 50-Ω load is placed at C2 terminal, and only the C1 terminal is connected to the coil.
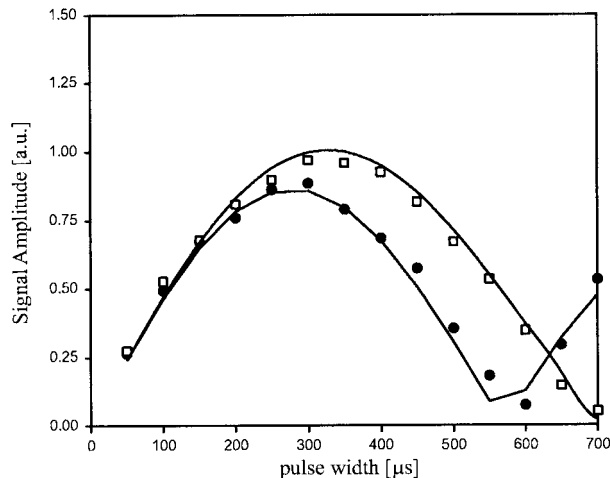
FIG. 5. Experimental and simulated signal amplitudes for a single pulse CP and LP excitation. The symbols indicate the experimental signal amplitudes for (●) CP and (□) LP; the curves are simulated. The LP signal was induced and detected by removing one of the two channels. The CP signal was induced using both channels driven in quadrature. The plot shows the CP signal acquired from one of the two channels. The simulations used $\omega_1/2\pi = 984$ Hz for both LP and CP modes.

($B_1 = 3.2$ G). For CP excitation the signals from the two modes were acquired separately.

The simulations used the density operator dynamic equations of Eqs. [27] and [35]. Inhomogeneous dephasing from an 800-Hz Lorentzian distribution was included during the RF pulses and free evolution time periods. Relaxation with parameters $T_1 = 16$ ms and $T_2 = 8$ ms was included during the time evolution delays.

Figure 5 shows the experiment and simulation results for single pulse LP and CP excitation experiments. For the CP results the signal from only one of the two channels is plotted. The maximum CP signal intensity is lower compared to the maximum LP signal; however, by combining the CP signal from the two channels, a final SNR gain of 1.2 is observed for CP excitation.

A two-pulse sequence was used to excite the echo signal. The optimum FID excitation pulse (300 μs for CP and 350 μs for LP) was used for the initial pulse. Following a free evolution delay of 1.5 ms, a second pulse refocused the signal into an echo. A two-step phase cycle was used where the phase of the first pulse was shifted in consecutive scans by π; this allowed phase cycling to remove the FID signal while keeping the echo signal. Figure 6 shows the echo signal amplitude as a function of the refocusing pulse width. Unlike the case of the FID signal intensities, the maximum CP excitation echo signal in one of the two CP channels is equal in intensity to the LP excitation echo amplitude. Combining the two CP channels, an overall increase of $\sqrt{2}$ in SNR can be obtained for CP excitation.

For both the FID and the echo experiments, CP excitation used twice as much power as LP excitation. Thus, as men-
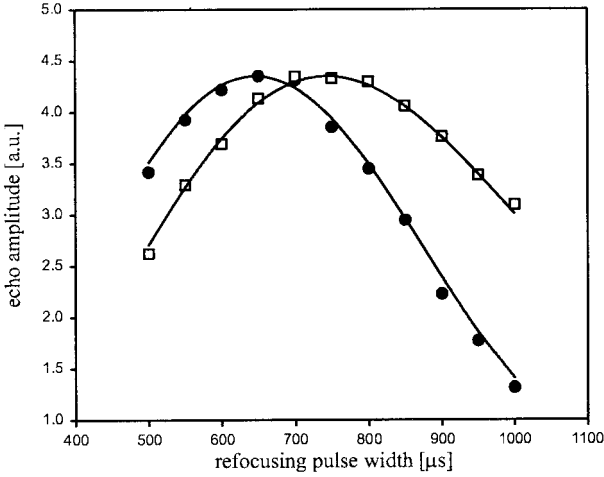
FIG. 6. Experimental and simulated echo signal amplitudes for two pulse CP and LP excitation. The symbols indicate the experimental signal amplitudes for (●) CP and (□) LP; the curves are simulated. A delay of 1.5 ms was used between the two pulses. The excitation and detection were done in the same manner as for the single pulse FID experiment. The simulations used $\omega_1/2\pi = 984$ Hz for CP mode and $\omega_1/2\pi = 1046$ Hz for LP mode.

tioned previously, for the same RF power levels, the optimum pulses for LP excitation would be slightly shorter compared to those of CP excitation.

In all cases there is excellent agreement between experiment and simulation in the overall excitation profile curve shape and amplitude. We found, however, that although we measured $\omega_1/2\pi = 984$ Hz, the LP simulated curve for echo amplitudes better fit the experimental points if we used $\omega_1/2\pi = 1046$ Hz. This change in ω_1 mainly results in an overall shift of the curve along the pulse width axis with no noticible change in the shape of the curve. We attribute this discrepancy to variations in the high power 50-Ω loads used for terminating the quadrature hybrid in going to LP mode.

6. CONCLUSIONS

We have shown that in NQR, the generation of CP signal is due to the powder orientation dependence of the effective excitation field. For a single crystal sample, analytical and numerical calculations show that CP excitation results in an LP signal; a powder average over one of the Euler angles γ is required to obtain a CP NQR signal. This result differs from what has previously been reported for NMR and axially symmetric spin-3/2 NQR systems where CP excitation results in a CP signal for both powders and crystals. An increase in SNR in CP excitation is also a result of powder averaging and is dependent on the pulse sequence implemented. Experiments and simulations have shown increases of 1.2 and 1.4 for the FID and echo signals, respectively, from a powder crystalline sample. Unlike NMR, however, pulse widths for optimum NQR excitation at a set RF power level *increase* for CP excitation. In practical applications,

gains in SNR from CP excitation must be weighed against the loss in Q in coil designs that would allow for CP excitation and detection, since the solenoid coil designs used for LP excitation in general will have higher Q values than any other coil design.

APPENDIX

The fictitious spin-1/2 operators (2) are defined as

$$I_{x,1} \equiv \frac{1}{2}\,I_x, \qquad I_{y,1} \equiv \frac{1}{2}\,I_y,$$

$$I_{x,2} \equiv \frac{1}{2}\,(I_yI_z + I_zI_y), \quad I_{y,2} \equiv \frac{1}{2}\,(I_xI_z + I_zI_x),$$

$$I_{x,3} \equiv \frac{1}{2}\,(I_z^2 - I_y^2), \qquad I_{y,3} \equiv \frac{1}{2}\,(I_x^2 - I_z^2),$$

$$I_{x,4} \equiv \frac{1}{2}\,(I_{y,3} - I_{z,3}), \quad I_{y,4} \equiv \frac{1}{2}\,(I_{z,3} - I_{x,3}),$$

$$I_{z,1} \equiv \frac{1}{2}\,I_z,$$

$$I_{z,2} \equiv \frac{1}{2}\,(I_xI_y + I_yI_x),$$

$$I_{z,3} \equiv \frac{1}{2}\,(I_y^2 - I_x^2),$$

$$I_{z,4} \equiv \frac{1}{2}\,(I_{x,3} - I_{y,3}), \qquad [42]$$

where

$$I_{x,3} + I_{y,3} + I_{z,3} = 0. \qquad [43]$$

They have the following commutation relations:

$$[I_{p,i},\, I_{p,j}] = iI_{p,k}, \quad i,\, j,\, k \text{ cyclic}$$
$$[I_{p,i},\, I_{p,4}] = 0 \qquad [44]$$

and trace property:

$$\mathrm{tr}[I_{p,i}I_{p,i}] = \frac{1}{2}, \quad i = 1,\, 2,\, 3. \qquad [45]$$

ACKNOWLEDGMENTS

REFERENCES

1. A. Abragam, "Principles of Nuclear Magnetism," Clarendon Press, Oxford, 1961.

2. R. S. Cantor and J. S. Waugh, Pulsed spin locking in pure nuclear quadrupole resonance. *J. Chem. Phys.* **73,** 1054–1063 (1980).

3. C.-N. Chen, D. I. Hoult, and V. J. Sank, Quadrature detection coils—A further $\sqrt{2}$ improvement in sensitivity. *J. Magn. Reson.* **54,** 324–327 (1983).

4. C. E. Hayes, W. A. Edelstein, J. F. Schenck, O. M. Mueller, and M. Eash, An efficient, highly homogeneous radiofrequency coil for whole-body NMR imaging at 1.5 T. *J. Magn. Reson.* **63,** 622–628 (1985).

5. M. C. Leifer, Resonant modes of the birdcage coil. *J. Magn. Reson.* **124,** 51–60 (1997).

6. J. B. Miller, A. N. Garroway, and B. H. Suits, NAR detection: Seeing more of what is there. Presented at the 40th Rocky Mountain Conference, 1998.

7. S. Vega and A. Pines, Operator formalism for double quantum nmr. *J. Chem. Phys.* **66,** 5624–5644 (1977).

8. M. J. Weber and E. L. Hahn, Selective spin excitation and relaxation in nuclear quadrupole resonance. *Phys. Rev.* **120,** 365–375 (1960).